Efficiency of the Use of Commercial Superhydrophobic Coatings in the Fields of Marine Industry

A. I. Ukolov[a], * and T. N. Popova[a]

[a] Kerch State Marine Technological University, Kerch, Republic of Crimea, 298309 Russia
***e-mail: Ukolov_aleksei@mail.ru**

Abstract—The antifouling and condensation properties of the Rust-Oleum Neverwet and Ultra Ever Dry systems have been experimentally studied in order to employ the effect of superhydrophobicity under marine conditions. The experiments have shown that the deposited coatings hinder the appearance of first colonies at contact angles $\theta_C \geq 130°$. The rate of condensation on a superhydrophobic surface is increased by 8–13% relative to that on an untreated surface. However, at the initial stage, the increase in the condensation rate is due to the larger specific area of the rough surface as compared with the smooth surface. A high heat-transfer coefficient can be provided by the transition of droplets into the Cassie–Baxter state, with this transition depending on the texture of a surface and the properties of water vapor. Nevertheless, there are substantial problems that must be solved to make such coatings applicable. First, their microstructure must be rather strong to withstand the conditions of a marine medium. Second, the coating must remain superhydrophobic for a long time. Additional studies and elaborations must be carried out before employing superhydrophobic coatings under real conditions.

1. INTRODUCTION

In recent years, the methods of formation and characteristics of superhydrophobic (SH) surfaces have provoked a substantial scientific interest due to their application in practical fields, including self-cleaning [1], anti-icing [2, 3], antifouling, intensification of condensation, and decreasing adhesion and frontal drag [4–6].

Construction is one of the fields in which SH coatings are applied. In [7], a method has been proposed for the production and application of emulsions that make it possible to generate and regulate hydrophobic properties of concrete and other materials. This method enables one to produce superhydrophobic concretes with water-repellent properties, large contact angles, and small rolling angles. Such concrete can be used in construction as a highly durable material.

Of urgency is the problem concerning the application of the phenomenon of superhydrophobicity in the light industry. Le et al. [8] have reported that the surface of a cotton fabric can be modified with copolymers of glycidyl methacrylate and (fluoro)alkyl methacrylates. These copolymers impart superhydrophobic properties to fabrics, thus increasing their contact angles to 165° and decreasing water absorption to 24%. The obtained SH coatings are highly stable to the action of aqueous media, repeated laundering, and abrasive actions.

Biological applications of SH coatings are also actively studied. The effects of micro- and nanotextures on the bactericidal properties of a surface were studied in [9, 10] upon its contact with suspensions of *Escherichia coli* K12 C600 or *Klebsiella pneumoniae* 811 cells in a nutrient medium. An SH copper surface has exhibited an enhanced bacterial inactivation caused by the toxic action of both a hierarchically textured copper surface and a high content Cu^{2+} ions in the dispersion medium.

Most commonly, the studies of the influence of wettability on bacterial growth and, hence, the degree of fouling result in proposing new methods for obtaining superhydrophobic surfaces [11–15]. However, these results are difficult to realize in the practice of shipbuilding. Vessel hulls are assembled from steels of certain types, which possess corresponding physical characteristics. Hence, only SH coatings that have adhesion to the necessary materials can be proposed to be used for the protection of such surfaces from biological fouling. The antifouling effect of an obtained surface must also be thoroughly verified. The majority of the authors analyze only the initial colonies under laboratory conditions with the use of artificial bacteria and sea water [12, 13, 16]. This does not always enable one to correctly predict the behavior of a protective

layer under real marine conditions. Sets of bionts are original and depend on many factors.

Another important application of SH coatings is the activation of condensation in heat exchangers employed on ships. Condensation is an integral component of various processes occurring in energy systems, which are characterized by high heat-transfer coefficients owing to the direct contact of a vapor with a solid surface. The rapid removal of droplets from a surface is of great importance for such systems [17–19]. Works [20–22] were the first scientific communications devoted to the dropwise condensation on superhydrophobic surfaces. The dropwise condensation comprises occurrence of several cycles. Each cycle consists of four processes, namely, the nucleation, growth, and coalescence of droplets followed by their detachment from a surface [23, 24]. Among these four processes, the rapid detachment of droplets can markedly increase the heat transfer. If a surface has a small hysteresis of the contact angle, the heat transfer is improved due to the easy removal of droplets.

Miljkovic et al. [25] have shown a 25% increase in the heat flux and a 30% increase in the heat-transfer coefficient of condensation on a nanostructured surface as compared with those on a smooth polymer surface at a supersaturation lower than 1.12. The authors have explained this finding by a coalescence-induced jump. The self-organized jump leads to a one–two orders of magnitude smaller size of an escaping droplet as compared with that in the slipping regime [26, 27]. Zhu et al. [28] have performed condensation experiments in a vaporous medium at a partial pressure of 3–7 kPa. They have shown a 125% increase in the heat transfer of condensation on a nanostructured surface, as compared with that on a smooth polymer surface. The enhancement of the heat transfer is explained by not only the coalescence-induced jump, but also an increase in the number of sites of droplet nucleation. An analogous conclusion was inferred by Kim and Nam in [29], where they reported a 60% increase in the heat transfer from a nanostructured surface.

Having analyzed the experience of the use of previously obtained data, we decided to make use of the opportunity to study the influence of superhydrophobicity on the fouling and condensation under real marine or coast conditions.

2. EXPERIMENTAL

2.1. Materials and Investigation Methods

Experiments were carried out using metals and alloys applied in the shipbuilding and heat supplying systems, namely, A40S, D40S, and A32 steels and AMg6 aluminum–magnesium alloy. The surfaces of the samples were preliminarily ground while gradually decreasing abrasive grits. Finishing mechanical polishing was performed with a chromium oxide (Cr_2O_3)

dispersion in pure kerosene until a mirror surface was obtained.

A superhydrophobic layer was formed on an experimental substrate via aerosol sputtering of a two-component system by the pneumatic method. Rust-Oleum®, Neverwet®, and Ultra Ever Dry® commercial hydrophobizing systems, which are applied to prepare SH surfaces on metal and nonmetal materials, were used in the experiments to provide samples with the roughness to make them nonwettable [30–32]. A basic layer, which contained methyl isobutyl ketone, butyl acetate, and mineral alcohols, was, first, applied onto a sample surface by uniform sputtering two or three times from a distance of nearly 15 cm for 3–4 s. Then, the layer was dried under normal laboratory conditions for 30 min. Thereafter, an external coating was formed by sputtering silica (SiO_2) particles suspended in acetone. According to manufacturer's data the used silica particles had sizes of 40–100 nm. The surface was dried under ordinary laboratory conditions for at least 12 h before the examinations.

The images of the surface structures of the SH layers were obtained using an SZM7045T-B1 optical microscope, which was equipped with an HDMI VGA 18MP HD USB TF video ocular and connected with a computer. The sizes of the surface structures were determined with a profilometer of the 130 model (Proton, Russia), which measured roughness with a high accuracy (resolution in the z direction is 4 nm). Four roughness parameters were measured (arithmetic average deviation R_a of the profile, quadratic roughness R_q, height R_z of profile asperities at ten points, and total height R_t of the roughness profile).

Contact angle θ_C (Fig. 1a) and the difference between advancing θ_{adv} and receding θ_{res} angles (contact angle hysteresis) are the quantitative characteristics of wettability. The value of droplet contact angle θ_C is related to the interfacial energies at solid–liquid (f_{SL}), solid–vapor (f_{SV}), and liquid–vapor (f_{LV}) interfaces via the following expression:

$$\cos\theta_C = \frac{f_{SV} - f_{SL}}{f_{LV}}. \qquad (1)$$

If a contact angle is $\theta_C < 90°$, the surface is hydrophilic, while contact angle $\theta_C > 90°$ corresponds to the hydrophobic interaction. An increase in the contact angle to $\theta_C > 150°$ and a decrease in the hysteresis to $\theta_{adv} - \theta_{res} < 10°$ indicate the passage to the superhydrophobic state.

To determine contact angles θ_C (Fig. 1a), the droplets were observed and photographed using a specially designed setup schematically represented in Fig. 1b [33, 34].

Light source *1*, through opal glass *2*, illuminated droplet *5* placed onto sample *4*, which was installed on holder *3*. All elements of the setup were mounted on an optical bench to make the images coaxial. Converg-
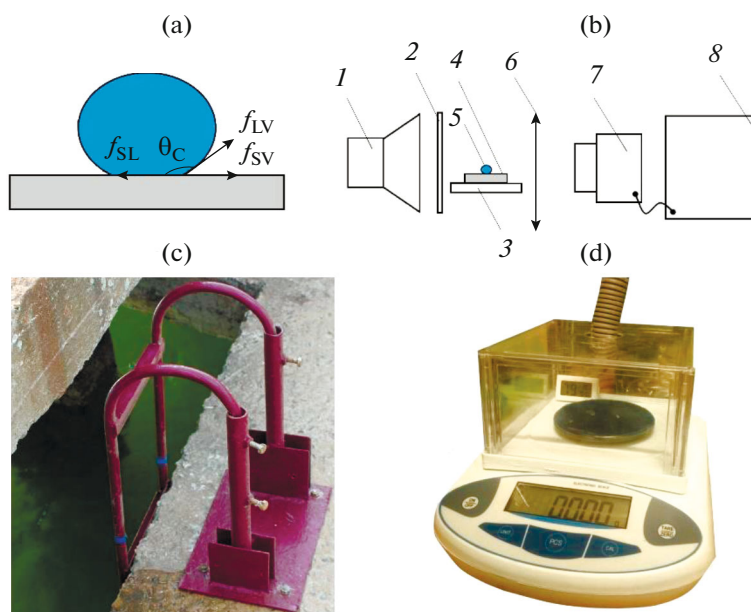
Fig. 1. (a) Droplet on an SH surface, (b) layout of a setup used to determine contact angles, (c) sample holder, and (d) setup used to determine condensation rate.

ing lens *6* and Canon EOS 550D digital photographic camera *7* connected to computer *8* recorded the water droplet located on the substrate. The droplet image was recorded after optical magnification with a viewfinder in real time. The obtained images were analyzed graphically with the help of the sPlan 7.0 software.

The contact angle hysteresis was determined using the inclined plane method [35]. According to this method, the images of the droplet profile were recorded while the inclination of a substrate was increased, and the profile recorded immediately before the droplet began to move was used to determine the advancing and receding angles.

2.2. Immersion of Samples in Sea Water and Monitoring of Biological Fouling

This experiment was carried out for 3 months (August−October) in the Kerch Strait (45°16′15.0″ northern latitude, 36°25′18.0″ eastern longitude) and was repeated for 2 years. The samples were fastened in a special holder (Fig. 1c) installed on a pier and immersed in sea water to a depth of larger than 1 m in August. The entire experiment was performed using 15 steel plates. The distance between their rows was 30 cm. One side of all plates was covered with a superhydrophobic layer. The opposite side was polished. The measurements of the contact angles, optical examinations, and collection of fouling samples for biological analysis were carried out every 7 days after the onset of the experiment.

The weather conditions were recorded daily at the same time moment (at 12:00) during the entire period of the experiment. The temperatures of air (25.4−32.3°C) and water (23.9−26.4°C) remained to be rather stable. The maximum wind velocity was 10−12 m/s at an average value of 6.48 m/s throughout a period of observations.

Detailed information on the fouling composition was obtained with the help of microscopic examinations performed using a Zoom SZM-45T2 stereomicroscope equipped with a Microscope DCM130 digital photographic camera. The sizes of attached microorganisms were determined optically from the difference between the counts of the micrometer screw by successively focusing the objective at different points of the thallus. The area of the fouling was determined graphically by superimposing a millimeter grid onto an image and calculating the ratio between the nodes located in the fouled and clean regions.

When taking samples for biological analysis, they were placed into a vessel with water to prevent the organisms from death. In the laboratory, the organisms were washed away with water on a classifying sieve, while their larger attached forms were separated with pincers. The samples were handled no later than 3 h after being taken, and a part of a mixture with organisms was examined in a Petri dish at an eightfold magnification. The microorganisms taken with pincers were placed into a test tube containing a 4% formalin solution. An analyzed sample was sorted into systematic groups down to families. The number of organisms of a given type was determined by direct counting of individuals in a sample.
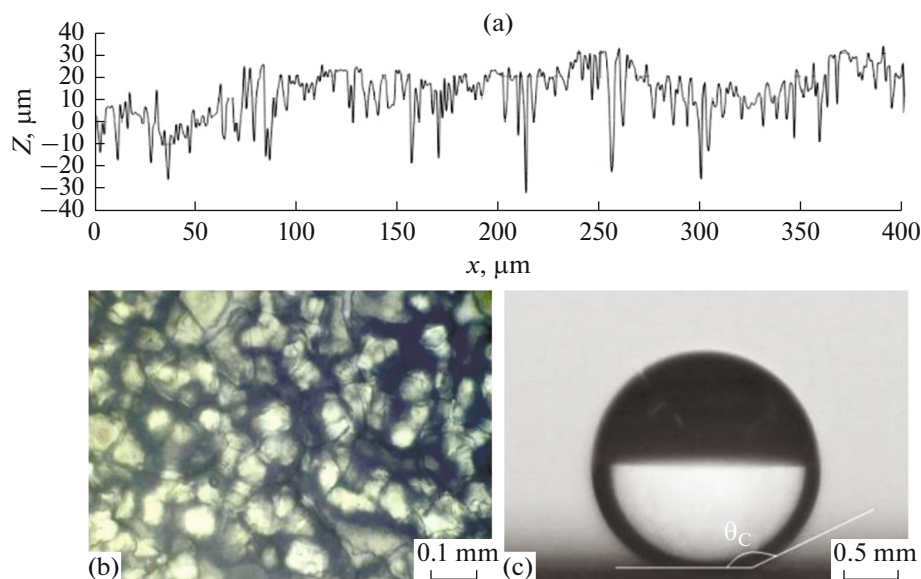
Fig. 2. (a) The cross section of the roughness profile determined with a profilometer for the entire surface, (b) optical microscopic image, and (c) droplet in the Cassie−Baxter state on a NeverWet SH surface.

2.3. Condensation on an SH Surface

2.3.1. Atmospheric water vapor. A40S shipbuilding steel plates with sizes of $8 \times 90 \times 50$ mm were used in the experiments. The samples were cooled to −5°C and placed under the objective of a SZM7045T-B1 microscope. The condensation process was recorded with the help of a HDMI VGA 18MP HD USB TF eyepiece in equal time intervals, while simultaneously measuring temperature with an HT-818 contactless two-beam IR laser thermometer. The temperature of ambient air was 20°C. The partial pressure of water vapor was 1400 Pa. The observations were continued until a sample was heated above the dew point and the condensation on its surface stopped. In the course of an experiment, air humidity determined by an OOT-DTY humidity meter was 59−60%.

2.3.2. Supersaturated solution. A special setup (Fig. 1d) was assembled to prepare a supersaturated solution and determine the condensation rate. Samples used to examine the temperature-induced condensation were placed onto a scale of a digital laboratory balance located in a closed box. The balance operated at an accuracy of 0.001 g. Water vapor was supplied into the box with a compressor-type humidifier at a rate of 0.28 mL/min. The shape of condensed droplets and the mass of the substance on the sample surface were recorded in the experiments.

3. RESULTS AND DISCUSSION

3.1. Coating Structure and Superhydrophobicity

The use of two types of materials for the deposition of SH layers has resulted in the formation of surfaces with the following characteristics.

Typical profiometry data on the NeverWet system are presented in Fig. 2a. The clusterization/agglomeration of particles present in a solution gave rise to a roughness with the arithmetic average and quadratic deviations of the profile $R_a = 12$ μm and $R_q = 15$ μm, respectively. The SH NeverWet system had total height $R_t = 127$ μm and height $R_z = 122$ μm of profile asperities. Semispherical asperities provided a roughness (Fig. 2b) necessary for the manifestation of the nonwettability effect and the passage of a droplet to the Cassie−Baxter state (Fig. 2c). For 5-μL droplets, the contact angle and hysteresis were $\theta_C = 153°$ and $\approx 5 \pm 2°$, respectively.

The use of the Ultra Ever Dry system provided lower roughness values $R_a = 6.7$ μm and $R_q = 8.2$ μm. The total height and asperity height of the profile were $R_t = 41.1$ μm and $R_z = 20.3$ μm, respectively (Fig. 3a). The surface was represented by microscopic islands separated by channels (Fig. 3b). For 5-μL droplets, the contact angle and hysteresis were $\theta_C = 150.3°$ and $\approx 7 \pm 2°$, respectively (Fig. 3c).

Thus, the stability of air captured in the pockets between microasperities was studied using mixtures having close chemical compositions but giving reliefs of different geometries. The NeverWet system led to a larger height of the roughness but a smaller average step of asperities as compared with those for the Ultra Ever Dry system.

3.2. Biological Fouling

Within the first 14 days, foulings were absent on the SH surfaces or were easily washed away with a flow of sea water. After a long-term exposure in water
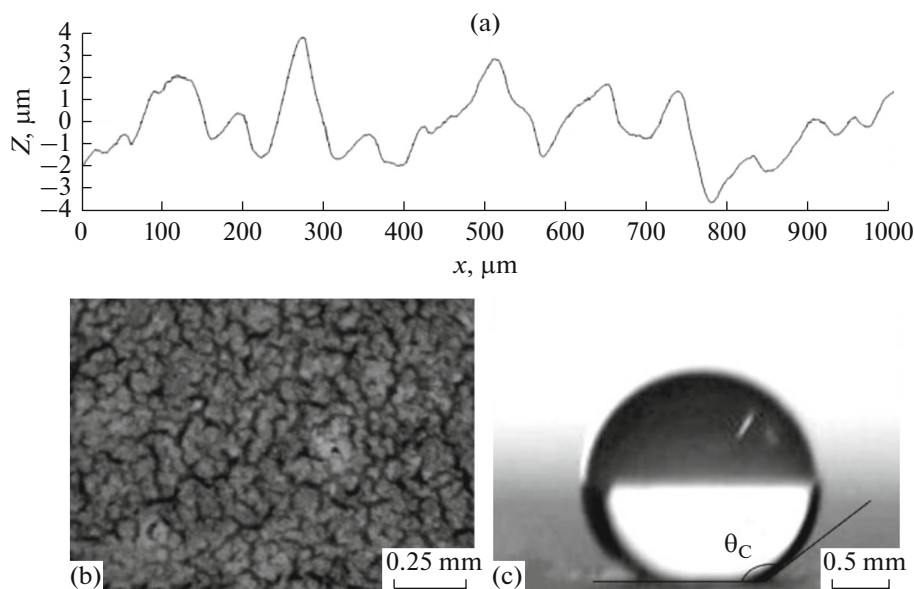
Fig. 3. (a) The cross section of the roughness profile determined with a profilometer for the entire surface, (b) optical microscopic image, and (c) droplet in the Cassie−Baxter state on an Ultra Ever Dry SH surface.

(21 days), the experimental plates were covered with green algae. The difference between the fouling volumes on the SH layer (Fig. 4a) and the opposite unprotected surface of a sample (Fig. 4b) was insubstantial; however, the thallus of the algae on the superhydrophobic coating had a smaller height. The deposition of hydrocole larvae and alga spores onto an intact substrate requires the formation of a bacterial film on its surface. The bacterial layer is formed faster on the hydrophilic (polished) surfaces than on the superhydrophobic ones. Larvae (spores) of foulings are deposited onto the hydrophilic surfaces faster and have larger sizes.

After 35-day exposure of the samples in water, the polished surface contained the foulings of the following groups (Fig. 4d): acorn shells (*Chthamalus stellatus*), sessile polychaete worms (*Serpula vermicularis*), pearlweeds (Bryozoa), and sponges (Porifera). Balanus (*C. stellatus*) was absent on the SH surface even after a 35-day test (Fig. 4c). Over the same time period, the size of fouling on the SH surface was smaller than that on the opposite side.

The quantitative criterion of the fouling was expressed as a change in the average volume of the microorganisms attached to the samples (Table 1). The initial state of a surface was taken to be the zero level. As the samples were exposed in water, the area and thickness of the fouling layer increased to maximum values, which were taken as 100%. On the polished surface, the maximum fouling volume was reached in 35 days. The fractions of fouling within other time periods were calculated for the surfaces of the two types relative to this value. In colder seasons, the fouling proceeded slower than in the summer−

autumn period. An average fouling volume comparable with that reached over 35 days in the warm season was reached in 55 days, when the samples were immersed in autumn.

It should be noted that the deceleration of fouling is not directly related to the effect of superhydrophobicity. The smaller volume of microorganisms is, most likely, associated with the chemical composition of an SH coating. The polished surface is rapidly oxidized and covered with the biocorrosion products, which are good substrates for other types of foulings. The main difficulty in the quantitative assessment of the effect of superhydrophobicity is the safety and stability of the air gap between a liquid and a solid, as well as the integrity of the structure of the SH coating. Our measurements of contact angle θ_C upon the long-term immersion of the samples in sea water indicated that their surface remained superhydrophobic for no more than 7 days. In 14 days, $\theta_C < 135°$. In 28 days, the hydrophobicity of the surface disappeared ($\theta_C < 88°$). Therefore, subsequent observations made no sense. Several reasons may be noted for the disappearance of the SH state. First of all, mechanical degradation of the surface roughness must be mentioned. Sea waves cause water oscillations at an SH coating, thereby wash away silica particles from the substrate of the layer. The wear is enhanced by small sand particles, which are present in sea water. They not only act as abrasive elements, but also contaminate the surface (Fig. 5a). The distortion of the relief makes the surface wettable and causes the appearance of initial fouling colonies.

Mechanical strength of SH coatings depends on their properties. The commercial systems used in the
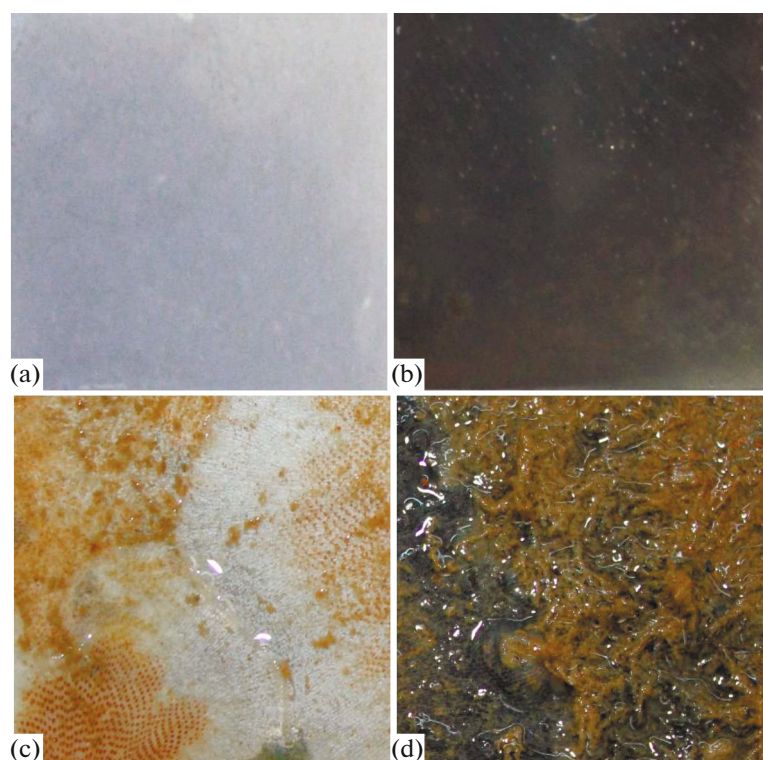
Fig. 4. (a) SH and (b) untreated surfaces before the test and (c, d) after 35-day exposure in water.

work exhibited a low resistance to viscous friction. The repetition of the experiments under laboratory conditions confirmed that the SH layers were washed away. Under the action of forced oscillations of a sample in even pure sweet water, the contact angle decreased, and, in 7 days, it was $\theta_C = 130°$ in the lower part of a sample (Fig. 5b). Under the experimental conditions, this fragment was always under water. Upon the oscillations, the upper part of the sample coincided with a variable water line. The action of the forces of viscous friction and surface tension enhanced the wear of the SH layer, thus leading to $\theta_C = 95.2°$ (Fig. 5c). The wave action had the lowest effect on the wettability in the central part of the sample, where the contact angle was 149.3° (Fig. 5d).

The strength of a material depends on its nature and the method of SH surface formation. Another problem concerning the stability of the air gap is of a more general character. One should distinguish between the states of air upon the presence of a droplet on an SH surface and when a sample is partly or completely immersed in water. When a gas layer between the asperities of an SH relief is in contact with atmosphere, its pressure is equal to the atmospheric one, and it is not subjected to an additional pressure of a liquid. Another situation arises upon the complete immersion. Critical hydrostatic pressure P_c may vary

Table 1. Average fouling volumes

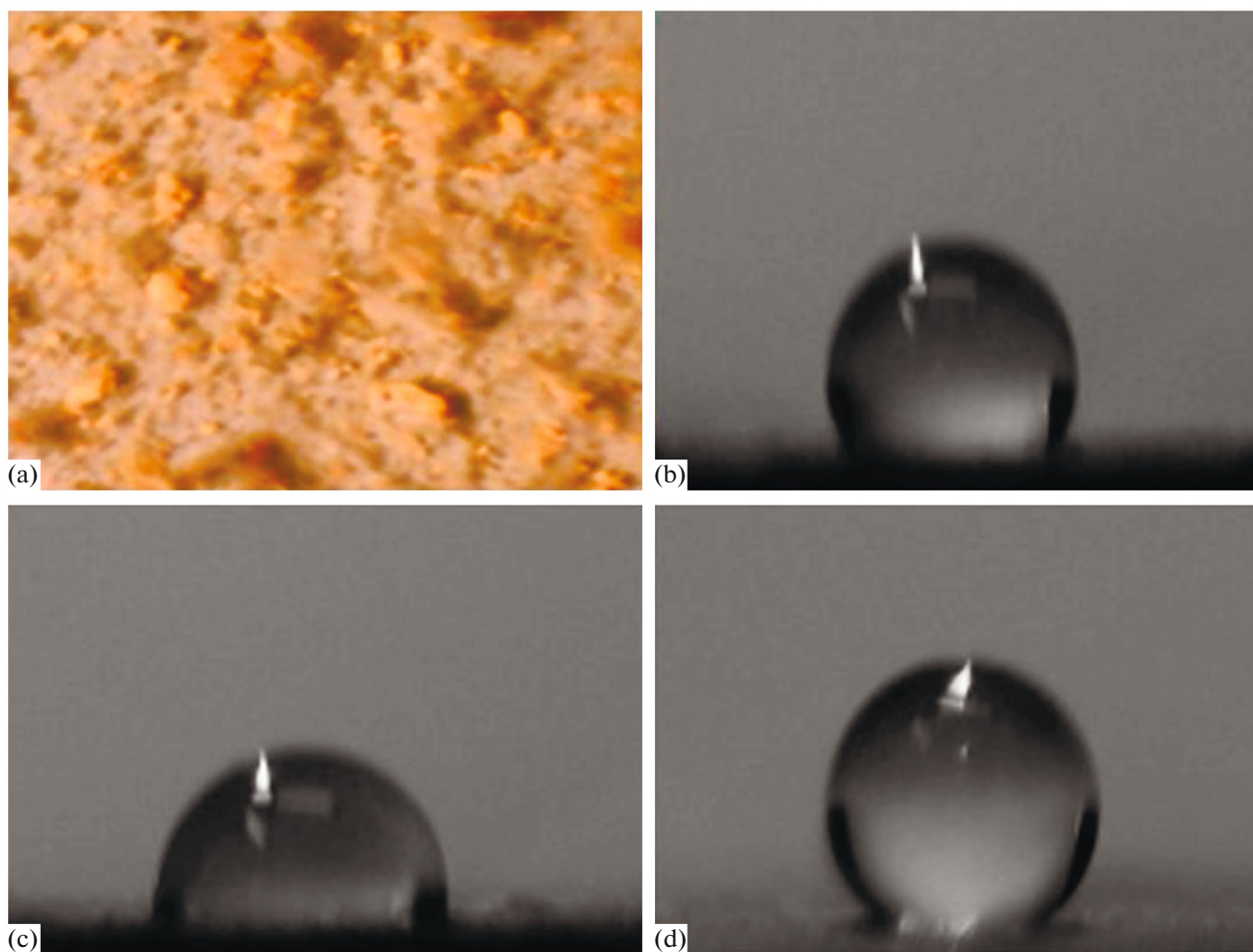| Days	SH		Polished	
	august−september	september−october	august−september	september−october
14	10 ± 2%	0%	17.5 ± 3%	6 ± 1.5%
21	22 ± 3%	8 ± 2%	30 ± 3%	13 ± 2%
28	55 ± 3%	30 ± 3%	78 ± 3%	42 ± 2%
35	89 ± 5%	53 ± 3%	100 ± 5%	64 ± 3%

Fig. 5. (a) Sand particles and (b–d) sea water droplets on an SH surface exposed to 7-day test in sea water subjected to forced oscillations in the (b) lower, (c) upper, and (d) central part of the sample.

within a range of 0.2–38.6 kPa depending on the methods of SH coating formation and investigation [36]. According to [37], the analytical equation of the critical pressure for SH surfaces consisting of ordered spherical particles is based on the force balance for a meniscus surrounding a given particle:

$$P\left(L_s^2 - \frac{\pi d_s^2}{4}\sin^2\alpha\right) = \pi\sigma d_s\sin\alpha\cos\left(\frac{3\pi}{2} - \theta - \alpha\right), \quad (2)$$

where d_s is the sphere diameter, L_s is the distance between the centers of two neighboring spheres, and α is the angle that characterizes the height of meniscus location. Then,

$$P_c = \frac{4\pi\sigma d_s\sin\alpha\cos\left(\frac{3\pi}{2} - \theta - \alpha\right)}{d_s\left[4\left(\pi/6\varepsilon\right)^{\frac{2}{3}} - \pi\sin^2\alpha_c\right]}, \quad (3)$$

where $\varepsilon = \frac{\pi d_s^2}{6L_s^2}$.

Our mathematical assessments implemented for the critical pressure by Eq. (3) on the basis of profilometry data have shown the existence of a boundary state. For $d_s = 2-10$ μm, $L_s = 6-10$ μm, contact angles $\theta = 150°-153°$, and $\sigma = 74.5$ mN/m, we have obtained interval $P_c = 8-25$ kPa, which coincides with the pressure in the natural experiment (10–13 kPa).

To make the situation more specific, we monitored the state of the air gap upon a gradual immersion of a sample in water to depth $h = 5-50$ mm. A sample prepared as a metal plate with an applied SH layer of the NeverWet system (Fig. 2) was placed into a transparent vessel filled with water (Fig. 6a, *1*). After the immersion, an air gap arises between the liquid and the solid. Water is brought in contact only with the tops of the SH layer relief. This state is denoted by the light background in Fig. 6b. The white spots correspond to air bubbles, which have been captured between the asperities of the SH coating. However, immediately after immersion, water starts to penetrate between the surface asperities beginning from a sam-
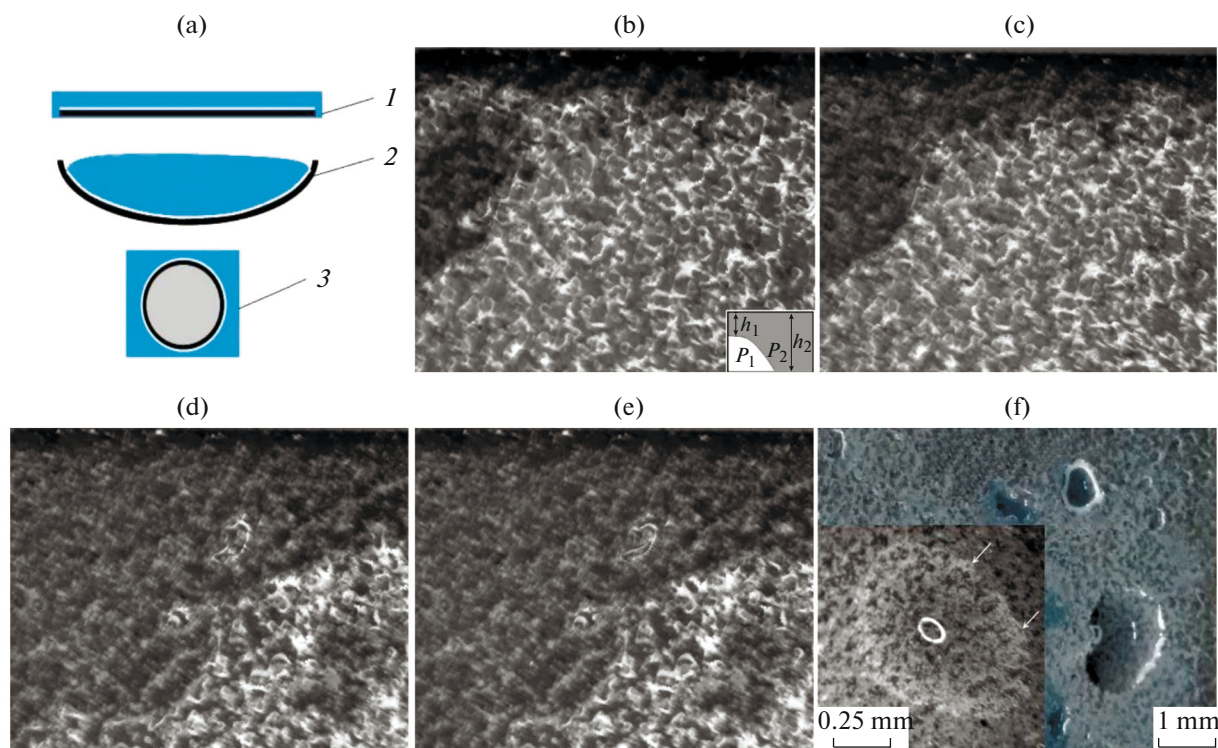
Fig. 6. (a) Variants of immersion in water and shapes of the samples; SH surface wetted beginning from a plate edge for (b) 10, (c) 30 s, (d) 12, and (e) 25 min (magnification of 35×); and (f) large air clusters on a watered SH surface.

ple edge. In Figs. 6b–6e, this region has the dark background.

In the first few seconds of the observation, the lateral wetting of the SH layer develops rather rapidly. The dynamic monitoring has shown the gradual filling of individual dents or their groups with water. Therewith, air does not escape through the liquid layer into the atmosphere. The penetration of water along the SH surface decelerates with time (Figs. 6c–6e). The next stage of surface wetting with water comprises the coalescence of small bubbles into larger ones (Fig. 6f). Due to the coalescence, air vacates the dents of the roughness, and water immediately penetrates into them. Large bubbles may detach from the surface and escape into the atmosphere. As a result, the entire SH surface is watered. This watering process is rather long and may last several days. A similar behavior was also observed upon the complete immersion for the Ultra Ever Dry coating. The only difference was the fact that, because of the roughness height of this coating, the air bubbles were thinner. Thus, the watering is independent of the geometry of the roughness asperities. After the samples were withdrawn, water remained between the microasperities and did not flow down upon inclination and even shaking. We failed to measure the contact angles under such conditions. After the surface was dried with a warm air flow,

the SH effect was restored and the measured contact angle was larger than 150°. Hence, the loss of the SH state was not caused by coating degradation.

The penetration of water into the dents between the SH relief asperities may be caused by the additional hydrostatic pressure. When a sample having an SH surface is immersed, the pressure gradient arises not only in the vertical, but also in the horizontal direction. The pressure drop in the direction parallel to the plate plane is related to the height of the air gap rather than height h of the water column (Fig. 6b, inset). If the SH layer has finite boundaries, height h_2 of water in the wetted region and, hence, pressure P_2 are higher than height h_1 over the air dent and pressure P_1, respectively. Pressure drop $\Delta P = P_2 - P_1$ can be easily estimated using the data on the surface roughness. For the two types of the SH systems, $\Delta P = 0.1-1$ Pa. However, this pressure drop is sufficient to induce a flow of $\approx 10^{-7}$ kg/s in the horizontal direction. This flow rate is comparable with the rate of watering the SH coating at the onset of the experiment.

The pressure gradient generated along the surface "forces" air out of the microdents to form increasingly larger clusters of the bubbles. To avoid the edge effect and the influence of the wetting regimes, the SH layer was immersed according to the scheme represented in
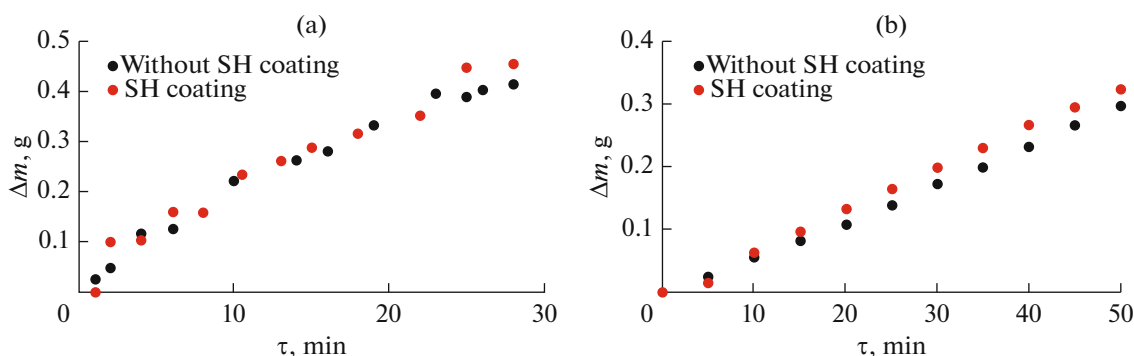
Fig. 7. Time dependences for the mass of condensed (a) atmospheric and (b) supersaturated vapor.

Fig. 6a (*2*). A semispherical socket with a maximum depth of 10 mm and a radius of 50 mm was made in a sample. After filling with water, the air layer remained preserved for 7 days. After a week of observations, the experiment was interrupted. The air layer and the SH surface were stable. In order to confirm the assumption that water penetrates into the dents between the asperities of the SH layer microrelief due to the pressure drop, an SH sphere was immersed according to the scheme depicted in Fig. 6a (*3*). The results obtained by these two schemes coincided with that obtained for the immersed plate. That is, in a short time (less than 6 min) four or five large air bubbles were formed on the SH sphere surface as is seen in Fig. 6e. The pressure in the large bubble compensated for the hydrostatic pressure. Therefore, this state was stable for a long time. However, a fragment of the sample is wetted with water and will be actively fouled under natural sea conditions.

3.3. Condensation

Heat transfer depends on the rates of condensation and removal of droplets from a surface. Figure 7 shows the $\Delta m = f(\tau)$ time dependences for the mass of the vapor condensed on a sample surface with and without an SH coating. The experiments on the condensation of atmospheric vapor on a cooled surface (Fig. 7a) and the condensation of supersaturated vapor at room temperature (Fig. 7b) have shown a higher rate of condensation on the SH coating. The plots presented in Fig. 7 reflect almost linear dependences, from which the $\Delta m = f(\tau)$ equations were obtained. For the atmospheric vapor on the samples with the SH coatings, $\Delta m = 0.0178\tau$; for the coating-free surface, $\Delta m = 0.0165\tau$. In the experiment on the condensation of supersaturated vapor at room temperature, the rates of condensation on the surface with and without the SH coating were $\Delta m = 0.0066\tau$ and $\Delta m = 0.0058\tau$, respectively. A similar relation was reproduced in experiments repeated many times. The condensation has a higher rate on a rough SH surface. We may quantitatively estimate the superiority of the SH surface as

1.08−1.13 times. These values are lower than those reported in the literature [25−29]. This is due to the low heat conductivity of the commercial SH systems used to obtain the coatings studied in this work. Nevertheless, the increase in the condensation rate on the SH surface has been confirmed for both methods of the realization of the phase transition.

However, the condensation rate initially increases, because the specific surface area of a rough structure is larger than that of a smooth one. Water must be rapidly removed to substantially increase the condensation rate. It is assumed that, being located on an SH surface, droplets will pass to the Cassie−Baxter state, and water removal will be accelerated. However, we have encountered some difficulties at this stage. In the course of atmospheric vapor condensation, droplets are nucleated between the asperities of a rough surface (highlighted in Fig. 8a). They may be distinctly seen due to the reflection of the microscope lamp. In the course of time, the droplets grow and begin to coalesce with each other. After the condensation process is completed (Fig. 8b), water covers entirely the surface, including the asperities of the SH layer relief. The droplets do not pass to the Cassie−Baxter state, but rather wet the surface. In this state, the removal of water is strongly hindered, and the condensation decelerates. After the surface is dried and a droplet is once more applied, the surface exhibits the SH properties again (Fig. 8c). Thus, the watering of the surface is not associated with the irreversible degradation of the SH coating, but rather is due to the rapid hydration of the surface groups inherent in these commercial coatings.

Water condensation from air on a solid surface consists in the transition of water vapor to the liquid state via the formation of droplets followed by their coalescence into larger ones. The possibility of condensation is determined by the radius of a droplet nucleus relative to its critical value:

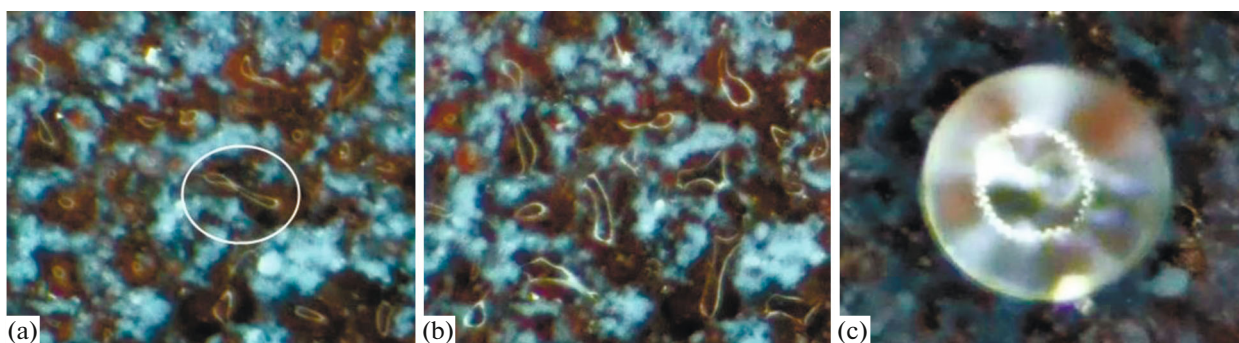$$r_{cr} = \frac{2\sigma\mu}{\rho N_A k T \ln S}, \tag{4}$$

Fig. 8. SH surface after condensation of atmospheric water vapor for (a) 9 and (b) 30 min, and (c) water droplet placed onto the dried surface; magnification of 35×.
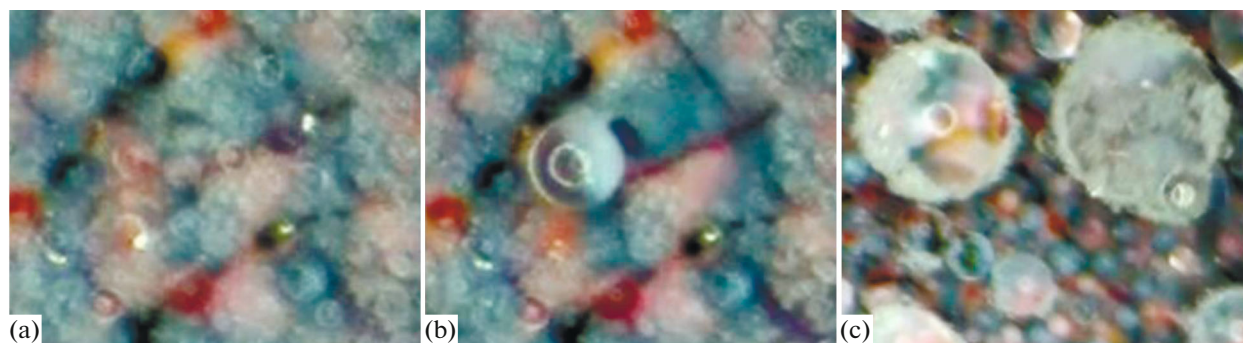

Fig. 9. Surface (a) before and (b) after the formation of a droplet in the Cassie−Baxter state and (c) SH coating debris on droplet surface; magnification of 35×.

where μ is the molar mass of water; ρ is the water density; N_A is Avogadro's number; k is the Boltzmann constant; T is the thermodynamic temperature of the existence of the phases; and S is the degree of vapor supersaturation, which is numerically equal to the ratio between the vapor pressure and the saturation vapor pressure at a given temperature. Hence, if the droplet radius is larger than r_{cr}, vapor will be condensed on it; if the droplet radius is smaller than r_{cr}, the droplet will be evaporated. The numerical analysis performed by Eq. (4) has given a critical radius equal to a few nanometers. According to the profilometry data, the arithmetic average distances between the roughness elements are 2 and 10 μm for the NeverWet and Ultra Ever Dry systems, respectively. Hence, the nucleation radius is many times smaller than the distance between the microasperities of a rough surface. Vapor will be condensed in the dents, accumulated, and clustered, thus wetting the region between the asperities of the relief. The transition to the Cassie−Baxter state during condensation was observed only in an experiment with supersaturated vapor on the NeverWet system. A compressor-type aerator creates a cloud of water droplets with sizes of 1−5 μm. This value is comparable with the distance between the

asperities of the NeverWet SH coating, and a jump-wise transition of the droplets to the Cassie−Baxter state has been observed for it (Figs. 9a, 9b).

One more problem is the degradation of an SH coating in the course of condensation. The nucleation, growth, and coalescence of small droplets distort the SH coatings. Droplets shift and destroy the microasperities of an SH layer. The forces of the interaction between small droplets and their attraction to large droplets exceed the adhesion forces of the micro/nanoasperities of an SH layer. The surface energy, which is released when two droplets coalesce, is not transformed into the kinetic energy of their jump or motion, but rather is consumed for the deformation and degradation of the SH layer. The separated fragments of the SH coating together with small droplets are absorbed by large droplets. Therefore, the next stage of condensation comprises the growth and simultaneous contamination of the droplets (Fig. 9c), which hinder their motion along the surface. As a result of the long-term condensation, the superhydrophobicity of the coating degrades, and the surface becomes hydrophilic. This process lasts nearly 40 min and is observed for both commercial systems and modes of vapor condensation.

4. CONCLUSIONS

The phenomenon of superhydrophobicity may be used as a promising method for optimization of technological processes in marine industry. In this work, we have considered the possibility of using the SH state for preventing marine objects from fouling and for accelerating condensation in heat exchangers. The study of the effect of wetting shipbuilding steel on its fouling under natural marine conditions has shown that a surface with a contact angle as large as 130° can be efficiently protected from the attachment of first bacteria and larvae. A bacterial film must be formed on the surface of a fresh substrate for the deposition of larvae and alga spores onto it. Such a bacterial layer is more rapidly formed on a hydrophilic (natural) surface of a shipbuilding steel than on a superhydrophobic surface. Thus, for an SH surface, a certain period is observed after which first colonies of organisms are attached to create a substrate for the formation of the next layer of fouling. The duration of this period depends on the time for which the surface can retain its hydrophobic properties at a level of $\theta_C > 130°$.

The control over vapor condensation enables one to make the processes occurring in heat exchanges more economically advantageous and efficient. The experiments have shown that the condensation rate on an SH surface is higher at the stage of water vapor deposition and at the stage of detachment of droplets, provided that they pass to the Cassie−Baxter state.

The phenomenon of superhydrophobicity will unambiguously be useful for practical applications in marine applications. The main problem concerns the development of a superhydrophobic state that would be stable for a long time. Watering and mechanical degradation are the main factors hindering the use of SH coatings under real operation conditions. Therefore, the improvement of the methods that would exclude the factors adverse for the formation of SH surfaces remains to be urgent.

CONFLICT OF INTEREST

The authors declare that they have no conflicts of interest.

REFERENCES

1. Kiiko, P.I., Chernykh, T.N., Ul'rikh, D.V., and Kriushin, M.V., *Izv. Vyssh. Uchebn. Zaved. Stroit.*, 2021, no. 6, p. 61.
2. Shilova, O.A., Tsvetkova, I.N., Krasil'nikova, L.N., Ladilina, E.Yu., Lyubova, T. S., and Kruchinina, I.Yu., *Transp. Sist. Tekhnol.*, 2015, vol. 1, no. 1, p. 91.
3. Krasil'nikova, L.N., Tsvetkova, I.N., Okovantsev, A.N., and Shilova, O.A., *Fiz. Khim. Stekla*, 2018, vol. 44, no. 6S, p.97.
4. Genzer, J. and Efimenko, K., *Biofouling*, 2006, vol. 22, p. 339.
5. Ferrari, M. and Benedetti, A., *Adv. Colloid Interface Sci.*, 2015, vol. 222, p. 91.
6. Samaha, M.A., Tafreshi, H.V., and Gad-el-Hak, M., *C. R. Mec.*, 2012, vol. 340, p. 18.
7. Kozhukhova, M.I., Flores-Vivian, I., Rao, S., Strokova, V.V., and Sobolev, K.G., *Stroit. Mater.*, 2014, no. 3, p. 26.
8. Le, M.D., Belukhina, P.O., Belukhina, O.O., Klimov, V.V., Bryuzgin, E.V., Navrotskii, A.V., and Novakov, I.A., *Izv. Volgograd. Gos. Tekh. Univ.*, 2017, no. 11, p. 117.
9. Emelyanenko, A.M., Kaminskii, V.V., Pytskii, I.S., Domantovsky, A.G., Emelyanenko, K.A., Aleshkin, A.V., and Boinovich, L.B., *Bull. Exp. Biol. Med.*, 2020, vol. 168, p. 488.
10. Boinovich, L.B., Kaminsky, V.V., Domantovsky, A.G, Emelyanenko, K.A., Aleshkin, A.V., Zulkarneev, E.R., Kiseleva, I.A., and Emelyanenko, A.M., *Langmuir*, 2019, vol. 35, p. 2832.
11. Pu, X., Li, G., and Huang, H., *Biol. Open*, 2016, vol. 5, p. 389.
12. Liu, T., Yin, B., He, T., Guo, N., Dong, L., and Yin, Y., *ACS Appl. Mater. Interfaces*, 2012, vol. 4, p. 4683.
13. Li, J., Wang, G., Meng, Q., Ding, Ch., Jiang, H., and Fang, Y., *Appl. Surf. Sci.*, 2014, vol. 315, p. 407.
14. Zhang, B., Li, J., Zhao, X., Hu, X., Yang, L., Wang, N., Li, Y., and Hou, B., *Chem. Eng. J.*, 2016, vol. 306, p. 441.
15. Sun, K., Yanga, H., Xue, W., He, A., Zhu, D., Liu, W., Adeyemi, K., and Cao, Yu., *Appl. Surf. Sci.*, 2018, vol. 436, p. 263.
16. Ekblad, T., Bergstrom, G., Ederth, T., Conlan, S.L., Mutton, R., Clare, A.S., Wang, S., Liu, Y., Zhao, Q., D'Souza, F., Donnelly, G. T., Willemsen, P.R., Pettitt, M.E., Callow, M.E., Callow, J.A., and Liedberg, B., *Biomacromolecules*, 2008, vol. 9, p. 2775.
17. Anikin, S.A. and Krivopalova, E.V., *Usp. Khim. Khim. Tekhnol.*, 2013, vol. 27, no. 6, p. 87.
18. Ashrafi-Habibabadi, A. and Moosavi, A., *Int. J. Heat Mass Transfer*, 2019, vol. 134, p. 680.
19. Sokuler, M., Auernhammer, G.K., Liu, C., and Bonaccurso, E., *Europhys. Lett.*, 2010, vol. 89, p. 36004.
20. Lafuma, A. and Quere, D., *Nat. Mater.*, 2003, vol. 2, p. 457.
21. Narhe, R.D. and Beysens, D.A., *Phys. Rev. Lett.*, 2004, vol. 93, no. 7, p. 76.
22. Wier, K.A. and McCarthy, T.J., *Langmuir*, 2006, vol. 22, p. 2433.
23. Sikarwar, B.S., Battoo, N.K., Khandekar, S., and Muralidhar, K., *Int. J. Heat Mass Transfer*, 2011, vol. 133, p. 216.
24. Xie, J., Xu, J., Li, X., and Liu, H., *Int. J. Heat Mass Transfer*, 2019, vol. 129, p. 86.
25. Miljkovic, N., Enright, R., and Wang, E.N., *ACS Nano*, 2012, vol. 6, p. 1776.
26. Boreyko, J.B. and Chuan-Hua, C., *Phys. Rev. Lett.*, 2009, vol. 103, p. 184501.
27. Gong, X.J., Gao, X.F., and Jiang, L., *Adv. Mater.*, 2017, vol. 29, p. 1703002.

28. Zhu, J., Luo, Y.T., Tian, J., Li, J., and Gao, X.F., *ACS Appl. Mater. Interfaces*, 2015, vol. 7, p. 10660.

29. Kim, H. and Nam, Y., *Int. J. Heat Mass Transfer*, 2016, vol. 93, p. 286.

30. Liu, H., Wang, Y., Huang, J., Chen, Z., Chen, G., and Lai, Y., *Adv. Funct. Mater.*, 2018, vol. 28, p. 1707415.

31. Gupta, R., Vaikuntanathan, V., and Sivakumar, D., *Colloids Surf., A*, 2016, vol. 500, p. 45.

32. Jiang, L., Park-Lee, K.J., Clinton, R.M., Tang, Z., Breedveld, V., and Hess, D.W., *Surf. Coat. Technol.*, 2017, vol. 328, p. 182.

33. Zhao, T. and Jiang, L., *Colloids Surf., B*, 2018, vol. 161, p. 324.

34. Ukolov, A.I. and Popova, T.N., *Ekol. Vestn. Nauchn. Tsentr. Chernomor. Ekon. Sotrudn.*, 2018, vol. 15, no. 2, p. 102.

35. ElSherbini, A.I. and Jacobi, A.M., *J. Colloid Interface Sci.*, 2006, vol. 299, p. 841.

36. Amrei, M.M. and Tafreshi, H.V., *Colloids Surf., A*, 2015, vol. 465, p. 87.

37. Emami, B. Bucher, T.M., Vahedi Tafreshi, H., Pestov, D., Gad-el-Hak, M., and Tepper, G.C., *Colloids Surf., A*, 2011, vol. 385, p. 95.

Translated by A. Kirilin